Experiments in Fluids 36 (2004) 515–527
DOI 10.1007/s00348-003-0664-3

Determining the hydrographic parameters of the surface of water from the image sequences of a CCD camera

C. R. Chou, J. Z. Yim, W. P. Huang

Abstract Water surface fluctuations were analyzed using image sequences from a CCD (charge coupled device) camera. Both regular and irregular waves were used for the study. A transfer function is obtained by comparing the gray scales of the image and results of "in-situ" wave gauge array measurements. The effects of non-uniform illumination within the wave basin are imbedded in the transfer function. Thus, the obtained transfer function is directly applicable to all other areas of interests within the wave basin. Estimated wave heights are all in qualitative agreement with those obtained through direct measurements. It is shown that the averaged relative error between these two wave heights is less than 16%.

1 Introduction

Measurements of ocean waves are often conducted using "in-situ" devices such as wave gauges and buoys. It may be said that the accuracies of these measurements are relatively high. Only with this assumption, the results of point measurements can be used for extrapolation to the whole area under consideration. However, this assumption is invalid for wave fields in regions where the underlying topography varies considerably, or where there are man-made constructions nearby. Under these circumstances, either the measurements have to be carried out in various locations repeatedly, or a large amount of instruments have to be used simultaneously. All these can be both time-demanding, as well as inefficient.

In recent years there has been considerable interest in applying the techniques of remote sensing for the study of ocean waves. As compared with the conventional methods, this technique has a clear advantage in that the spatial information of a large area can be obtained instantaneously. The instruments for remote sensing can be either deployed as land-based or mounted on aircrafts. Since no direct contact with the water surface is necessary, the instruments are not liable to the usual damage such as that caused by severe sea conditions, fishing activities and the passage of water vehicles. It is therefore an efficient and economic technique to monitor the sea state.

In earlier days, remote sensing of the ocean surface was carried out through photographic devices. The relative brightness on the photograph can be considered proportional to the intensities of the lights reflected from the water surface. This was utilized by Stillwell and Pilon (1974) and Sugimori (1975). The authors have shown that both the absolute wave-number spectrum as well as the directional information can be obtained from a single image. However, since the images of the waves were not taken consecutively, no temporal information of the wave field can be obtained. In later years, radar systems have been used to monitor the fluctuations of the water surface. Since these radar images were recoded in sequence at a specific rate, a three-dimensional spectrum can thereby be determined (Young et al. 1985). This kind of power spectrum describes the distribution of wave energy in both the wave-number and frequency domain (Senet et al. 2000b). However, the costs of this kind of operation are relatively high.

It should be mentioned that the intensity of the color level in the images depends on the wave slopes, not on wave heights (Gangeskar 2000). Thus, a suitable relation for the modulations of the optical densities in images and that of the slopes of the water surface must be derived. Because there are no wave properties measured by "in-situ" instruments that can be used for calibration, spectra estimated from images are often presented in dimensionless forms.

There is another problem in image processing. Land-based cameras are often installed in places wherever is convenient. In this way, the down-looking angles of these cameras are not perpendicular to the water surface. This can cause distortions of the images. Thus, a rectangular area in the images is in reality a trapezoidal one. That is to say, the actually observed region in the image will become wider with increasing distance away from the camera. The scales of the space coordinates are not constant, which then lead to errors in the determination of the wave-number spectrum (Sugimori 1975). To overcome this problem, the so-called ground control points were used by Senet et al. (2000b). The known locations of the control points were then used later to correct the coordinates of the images. These are the marked points at specific locations with known coordinates. With these ground control points, the coordinates of the images

Received: 22 July 2002 / Accepted: 3 June 2003
Published online: 19 March 2004

C. R. Chou, J. Z. Yim, W. P. Huang (✉)
Department of Harbour and River Engineering,
National Taiwan Ocean University, 2 Pei-Ning Road,
20224 Keelung, Republic of China
E-mail: paulhw@mail.ebtnet.net
Fax: +886-2-24633684

The authors wish to express their gratitude for the financial aid of the National Science Council, Republic of China, Project Nos. NSC-91-2611-E-019–008 and NSC-91-2611-E-019–007.

can be corrected. The authors then used the in-situ measurements to calibrate the wave slope spectrum. In this way, unlike previous studies, estimates of the magnitude of wave parameters were achieved by these authors.

With the advance of the computer technology, researchers have studied the possibility of using digitized images from video cameras to study the wave field. In principal, this method is an extension of the holographic method to the time domain. Since successive images were taken at a specific rate, temporal changes of the wave field can therefore be studied. Furthermore, camera devices of this kind are less expensive and relatively easy to operate, as compared with radar devices.

Jähne and Riemer (1990) and Klinke (1996) have used optical devices to study small-scale wind generated water surface waves. CCD cameras were mounted atop of a wind-wave flume in a vertical down-looking position, and the light sources were mounted at the bottom of the flume. Image processing is based on the analysis of the optical densities in the images. The quality, as well as the proper way to acquire them are therefore of vital importance. Jähne and Riemer (1990) found that when the illuminations are arranged in an inappropriate way, the observed intensities of the frames decrease with distance away from the light source. They have proposed an equation to resolve the problem of non-uniform variations of the light intensities. This equation takes into consideration the relation between the distances to the light source and the pixels on the image. Alternatively, a compensation wedge in front of the CCD camera can be used to resolve the same problem (Keller and Gotwols 1983).

In passing, it is noted that in all these studies, regions covered by the CCD camera images are rather small. The wave field studied by Jähne and Riemer (1990), for example, has an area of 66.35 cm × 47.28 cm. In Klinke (1996), the area is 15 cm × 20 cm. On the other hand, the area used for the analysis by Senet et al. (2000a) has a dimension of 12 cm × 36 cm. Through these studies, our understanding of both the internal, as well as external, structures of the wave fields was greatly improved. However, it must be pointed out that for engineering applications the regions of observation are too small. For this purpose, the region of interest must be, say, an order of magnitude larger than those previously considered.

With this in mind, we have conducted a series of experiments. The images in our studies cover a wave field which has an area of approximately 310 cm × 575 cm. To relate the photographic densities to wave heights, "in-situ" wave gauges were used. In the following, we further divide the rest of this paper into four parts. In Section 2, a brief description of the experimental setups will be given. The problem of non-uniform illuminations is dealt with in Section 3. In Section 4, we present our results in estimating the hydrographic parameters through image sequences. Both regular and irregular waves will be considered there. With a short summary in Section 5 we then close this paper.

2
Description of the experiments

The experiments were carried out in the multidimensional wave basin in the Ocean Engineering Laboratory of the Department of Harbor and River Engineering. The square wave basin has 50 ms on each side, and is 1.0 m in depth. For the experiments reported here, the water has a constant depth of 0.4 m. During the experiments, the basin bottom was always even, and no constructions were placed. It is hoped that in this way complicated wave phenomena can be avoided. A serpentine wave generator of piston type, consisting of 56 paddles, each of 50 cm width, is used to generate both regular and irregular waves. A total of 30 wave gauges were used to measure the actual surface fluctuations in the region of interest. These wave gauges were arranged in form of a rectangular array. The spacings between the wave gauges are, respectively, 0.4 and 0.8 m for the short and the long side of the array. A sketch of the arrangement of the wave gauges can be seen in Fig. 1.

A total of eight different periods, ranging from 0.6 to 1.3 s, were used for the regular wave (uniform wave train) experiments. Each wave has the same height and period, which can be also represented as sinusoidal waves. For each period of the wave train, six different wave heights were used. On the other hand, the irregular (random) waves were also studied. Sea waves appear with the characteristics of irregularity, which can be analyzed by assuming that they consist of an infinite number of sinusoidal waves with different periods and heights. All the irregular waves generated here have as targets the JONSWAP type of spectra of the form:

$$S(f) = \alpha(2\pi)^{-4} g^2 f^{-5} \exp\left[-\frac{5}{4}\left(\frac{f}{f_p}\right)^{-4}\right] * \gamma^{\exp[-(f/f_p-1)^2/2\sigma^2]} \tag{1}$$

where:

α	Phillips constant, (0.081)
f_p	Peak frequency
γ	Peak enhancement factor, (mean3.3)

$$\begin{aligned} \sigma and &= and 0.07 : f \le f_p \\ and &= and 0.09 : f > f_p \\ and &= and 0.09 : f > f_p \end{aligned} \tag{2}$$

This empirical spectrum was first proposed by Hasselmann et al. in 1973 after analyzing their JOint North Sea WAve Project results. It describes the sea state where active wind wave generation is in progress (Goda 2000). All the experimental conditions are listed in Table 1.

A CCD video camera was installed 7.4 m above the still water level. It has a downward looking angle of 23°. As pointed out by Gotwols and Irani (1980), a CCD camera is superior to the conventional video cameras because: (1) the transfer function for the brilliance of the images to the output signal is linear; and (2) the temporal response is not affected by the delayed partial images. Two steps were also taken to improve the quality of the acquired images. First, in ideal conditions the process in wave images acquisition should be free from noise. However, just like in any other measurements, noise is always present. A few possible sources of the noise may include: electronic noise from the video devices, non-uniform illuminations in the basin, bubble clouds due to breaking waves, and inho-

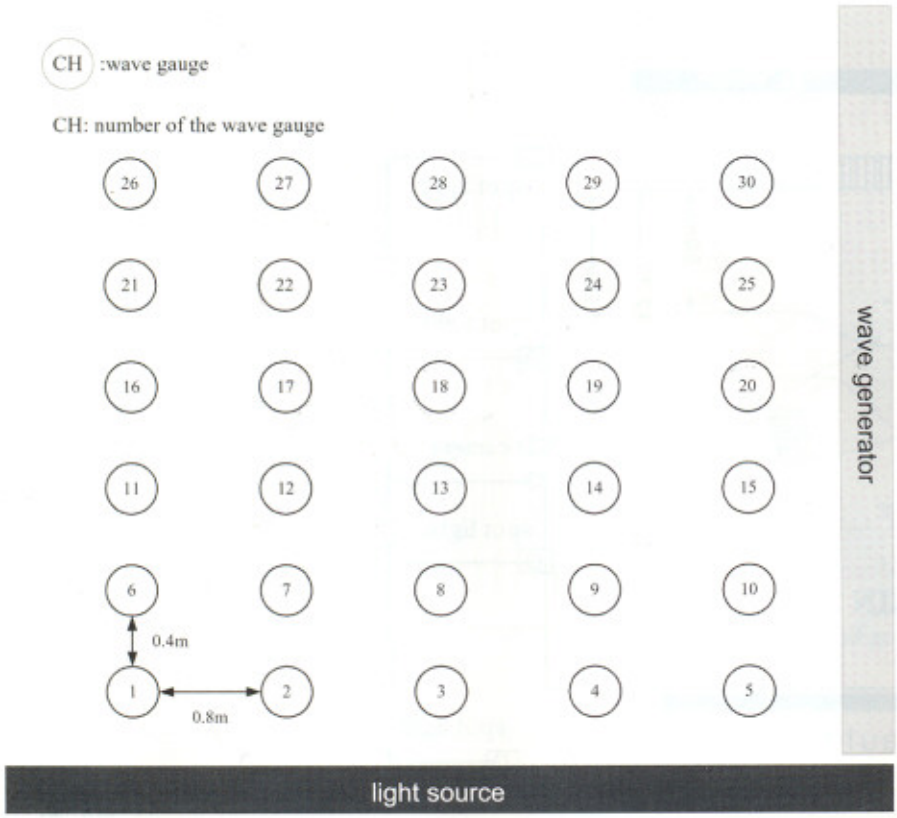

Fig. 1. Arrangement of the wave gauges

Table 1. The wave conditions of the experiments

	Wave Period (T) sec	Wave height (H) cm	Region–A	Region–B
			Numbers of wave height for each period	
Regular Waves	0.6	2.64–5.71	6	5
	0.7	3.42–6.74	6	5
	0.8	3.30–6.74	6	5
	0.9	3.41–6.42	6	5
	1.0	3.10–6.25	6	5
	1.1	2.72–5.77	6	5
	1.2	3.01–6.38	6	5
	1.3	3.10–6.29	6	5
Irregular Waves	$T_{1/3}$	$H_{1/3}$	Region–A	Region–B
	0.6	2.77–4.52	2	4
	0.7	3.19–5.62	0	4
	0.8	3.07–5.17	2	4
	0.9	2.76–5.74	0	4
	1.0	2.71–5.42	2	4
	1.1	2.89–5.36	0	4

mogeneous backgrounds of the surroundings (Jähne 1997). A polarized filter lens was placed in front of the CCD camera so that the effects of the lights scattered from the water surface can be minimized. Four spotlights were used for illumination. The heights of these light sources are the same as that of the camera. Second, there are four black tarpaulins placed along the 3 sides, and one atop of the wave basin. It is hoped that in this way, the effects of non-uniform reflections of the basin surroundings back to the camera can be minimized. A definition sketch of the experimental setups is shown in Fig. 2.

If the images were recorded in color, each pixel in the frame would be represented as a combination of the three basic colors, namely red, green, and blue, or the "RGB" values. It is considered that in this way there might be additional complications in the subsequent analyses. We have therefore decided to use a monochromatic format for the video signals. This means that reflections from water surface are represented in the images in the form of gray values. Accordingly, the color white is the brightest in the image and has a gray value of 255; whereas, the darkest is black and has a value of 0.

Water surface fluctuations were sampled at 20 Hz by the wave gauges. To be comparable, the images were first recorded in AVI format and then digitized by a frame grabber at a rate of 20 frames per second. The recording

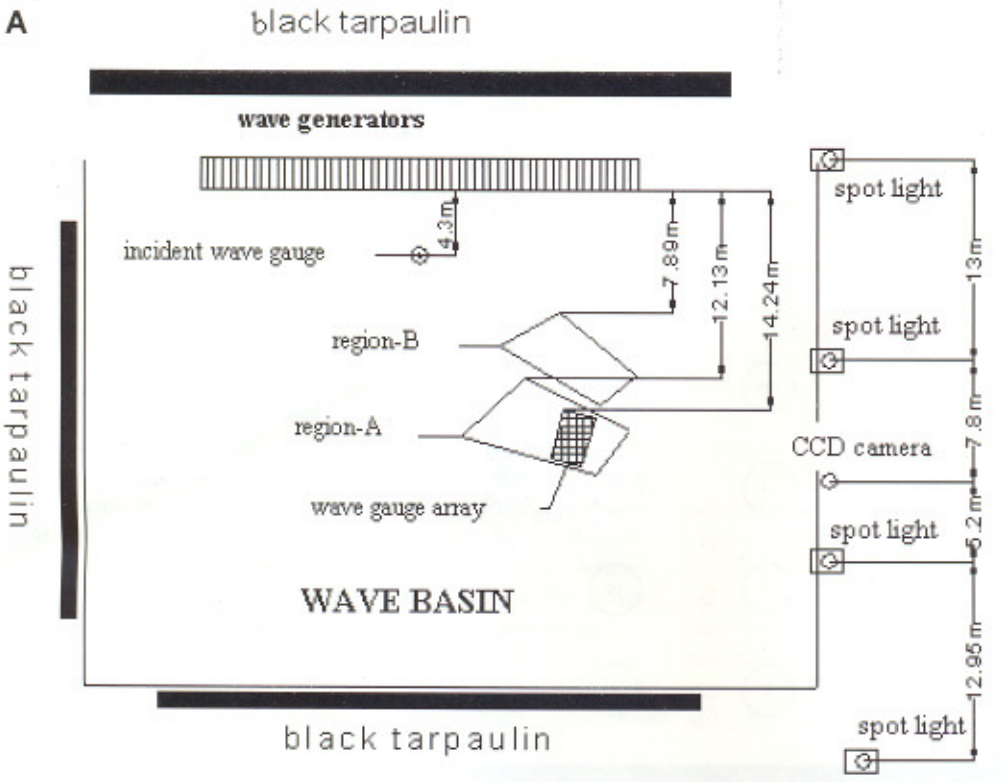

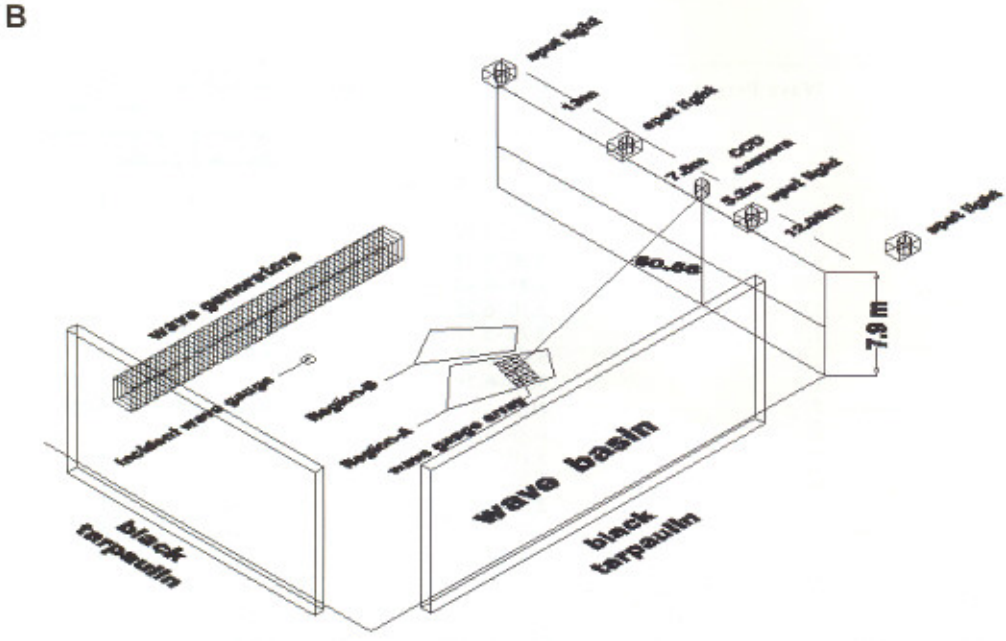

Fig. 2A, B. Set up of the experiments. **A** Top view. **B** Side view

length is 51.2 s for the cases with regular waves, and 102.4 s for those with irregular waves. It is believed that this can increase the reliability of the statistical estimates for the latter. The resolution of the wave images is 240 pixels 320 pixels per frame. As can be seen from Fig. 2, two regions in the basin were chosen for this study. Region A is of a trapezoidal form. It has a length of approximately 762 cm in the direction of the camera, and is 338 cm long in the transverse direction. Region B is similar in shape with Region A with a dimension of 310 cm by 575 cm. The relations between the characteristics of the wave fields measured by the wave gauges and those of the images in Region A are to be used for the estimation of the transfer function. Using the transfer function obtained from Region A, the gray values of the image sequences in Region B can be transformed into the characteristics of the waves. The results are then compared with those measured by the wave gauges as a verification of the transfer function. In this way, the feasibility of applying the transfer function in different regions can be assessed.

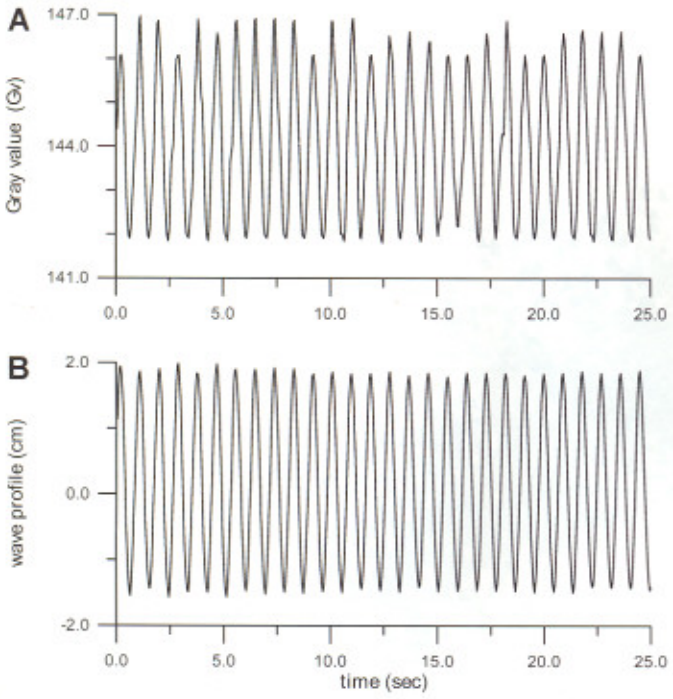

Fig. 3A, B. Time series Aof the gray value, and B of the wave profile

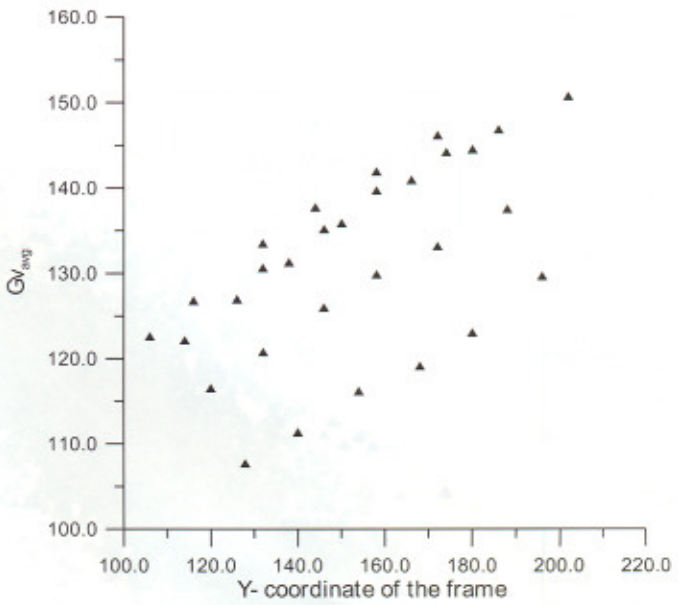

Fig. 4. Averaged gray value according to the ordinate of the frame

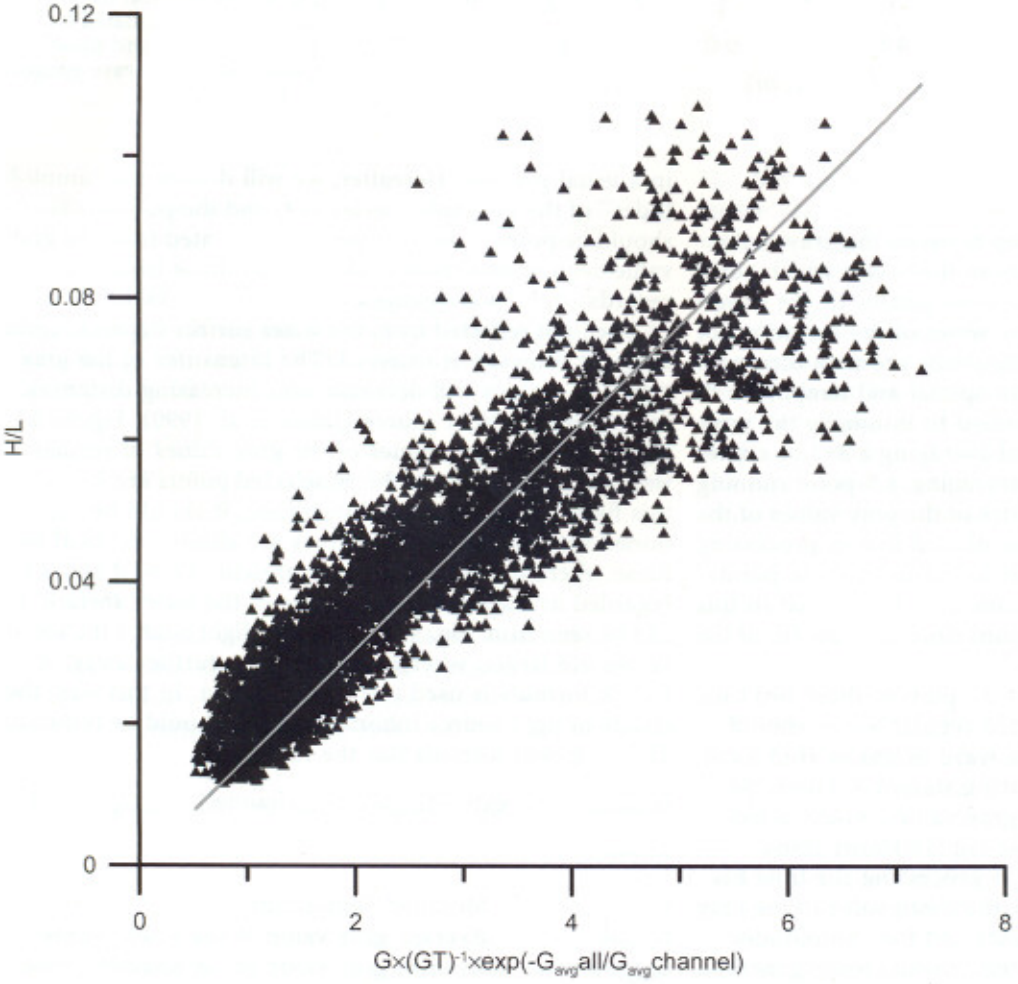

Fig. 5. Results of the goodness-of-fit test

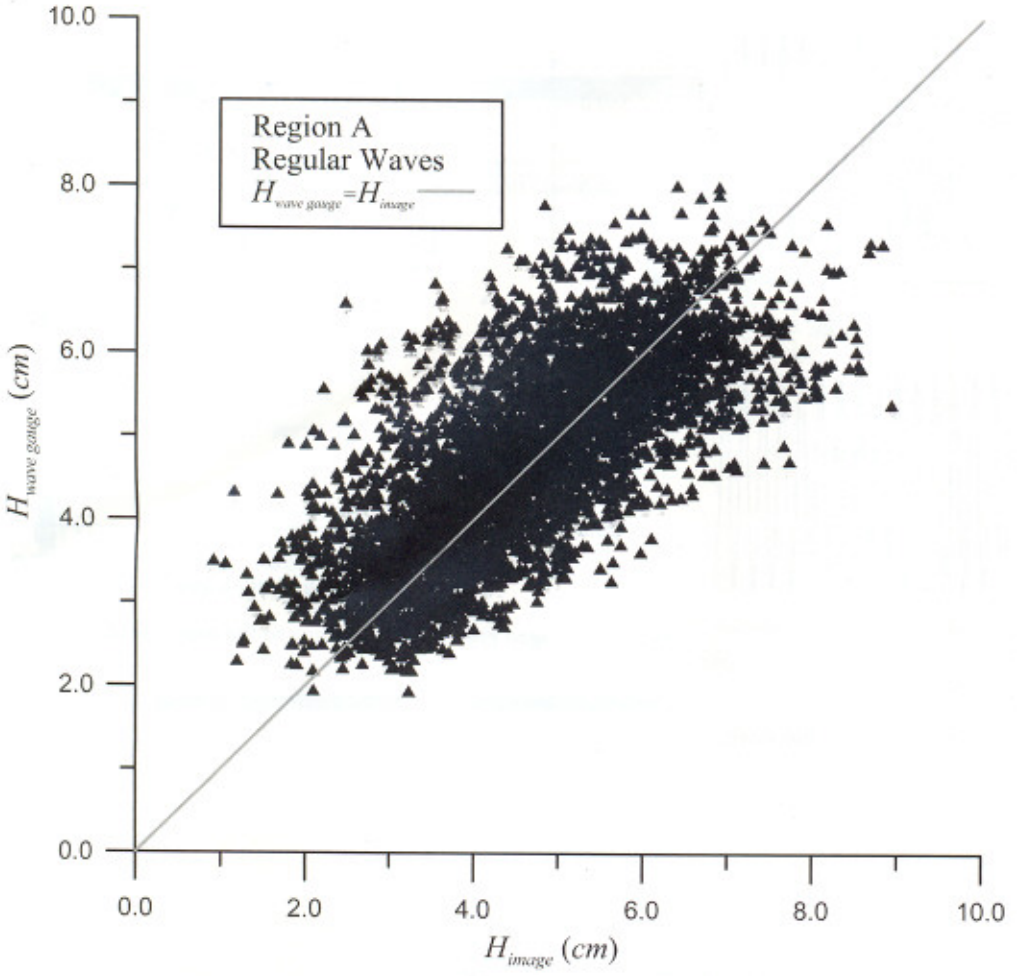

Fig. 6. Comparison of the wave heights estimated by the image sequence and those measured by the wave gauges of Region A

3
Data assimilation

To acquire the transfer function between the gray scales and wave characteristics, points in the image which correspond to the locations of the wave gauges in the wave basin were first identified. Time series of the variations of the gray scale values at these locations are then formed from the image sequences. Both spatial and temporal smoothing techniques were applied to minimize the possible effects of noise. For spatial averaging a 3×3 box-filter was used. As for the temporal averaging, a 5-point running average is used for the time series of the gray values of the selected points. It should be mentioned that in processing the data, the effects of different locations of these points were not taken into consideration. It is hoped that in this way, the effect of image distortions caused by the tilt of the camera could be reduced.

As an example, Fig. 3 shows the plots of these two time series for comparison. Generated regular waves should have a period of T=0.9 s and a wave height of H=3.5 cm. The data were from the measuring station 3. Figure 3a shows the time history of the gray values, as extracted from the image sequence, while Fig. 3b shows those measured by the wave gauge. In processing the time history from the image sequences, the mean value of the gray scale was subtracted. The periods and the "amplitudes" are then obtained by applying the zero-upcrossing method in a usual manner. Hereafter, we will denote the "amplitudes" of the gray value series as G and the period is G_T. It should be pointed out that periods estimated from the gray value sequences almost coalesce with those from the records of the wave gauges.

The light reflected from the water surface depends upon the light intensity it received. The intensities of the gray values in images will decrease with increasing distances away from the light source (Jähne et al. 1990). Figure 4 shows the averaged values of the gray values of regular waves. All the results of the 30 selected points are shown in this figure. Although not shown here, it should be mentioned that the mean gray values are almost identical to those where there are no waves present. Thus, it could be regarded as the background color of the water surface. It can be seen from Fig. 4 that near the light source the mean values are larger; whereas, it decreases further away. A simple formula is used for the correction. In this way, the effects of light source inhomogeneities should be reduced. The proposed formula has the form:

$$G_{\text{modified}} = G \cdot \exp(-G_{avg}all/G_{avg}channel) \qquad (3)$$

where:

$G_{modified}$	Modified "amplitude"
$G_{avg}all$	Average gray value of the whole frame
$G_{avg}channel$	Average gray value of the selected point

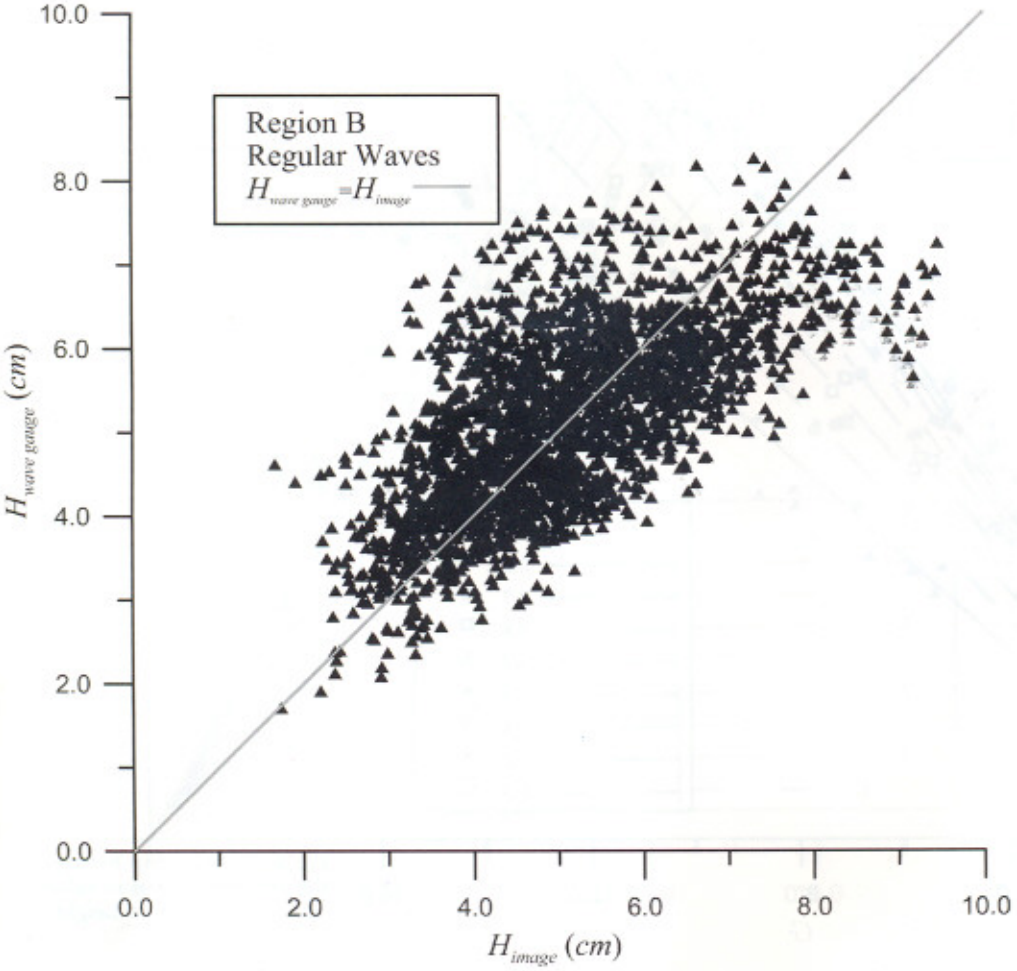

Fig. 7. Comparison of the wave heights estimated by the image sequence and those measured by the wave gauges of Region B

4 Results and discussion

4.1 Regular waves

Experiments with regular waves were carried out first. A relationship between the wave characteristics and the gray values can be obtained through regression:

$$HL^{-1} = 0.0145025 \cdot \left(G \cdot (G_T)^{-1}\right) \cdot \exp(-G_{avg}all/G_{avg}channel) \quad (4)$$

where:

H Wave height
L Wave length

The results are shown in Fig. 5, where values shown on the abscissa are estimated from the images, and those of the wave gauges are on the ordinate. Equation 4 can be rewritten in terms of wave heights and the modified gray scales as:

$$H = 0.0145025 \cdot \left(G \cdot (G_T)^{-1}\right) \cdot \exp(-G_{avg}all/G_{avg}channel) \cdot L \quad (5)$$

Figure 6 compares the two sets of wave heights as estimated through image sequences and the wave gauges. The data are from Region A. Values shown on the abscissa are the wave heights actually measured by the wave gauge arrays; whereas, those on the ordinate are estimated from image sequences via the transfer function. A straight line with a 45° inclination is also shown in the figure. When wave heights estimated from image sequences are equal to those measured by the wave gauges, they should fall on this line. It can be seen that the majority of the symbols are separated along the straight line, indicating that the predicted and measured wave heights are in the same trend. The mean value for the relative error is 0.157, where the relative error is defined as:

$$err = |H_{measured} - H_{estimated}|/H_{measured} \quad (6)$$

where:

$H_{measured}$ Wave height estimated from wave gauge records
$H_{estimated}$ Wave height estimated from the images

To test its universality, the transfer function was used for the images of Region B. The results are shown in Fig. 7. It is clear that for this case, the intensities of the reflections received by the camera must have been changed since the camera has now a different orientation than before. While the mean of the gray value for the whole frame is 130.99 for Region A, it is 125.36 for Region B. However, it can be seen that the transfer function still performs well in

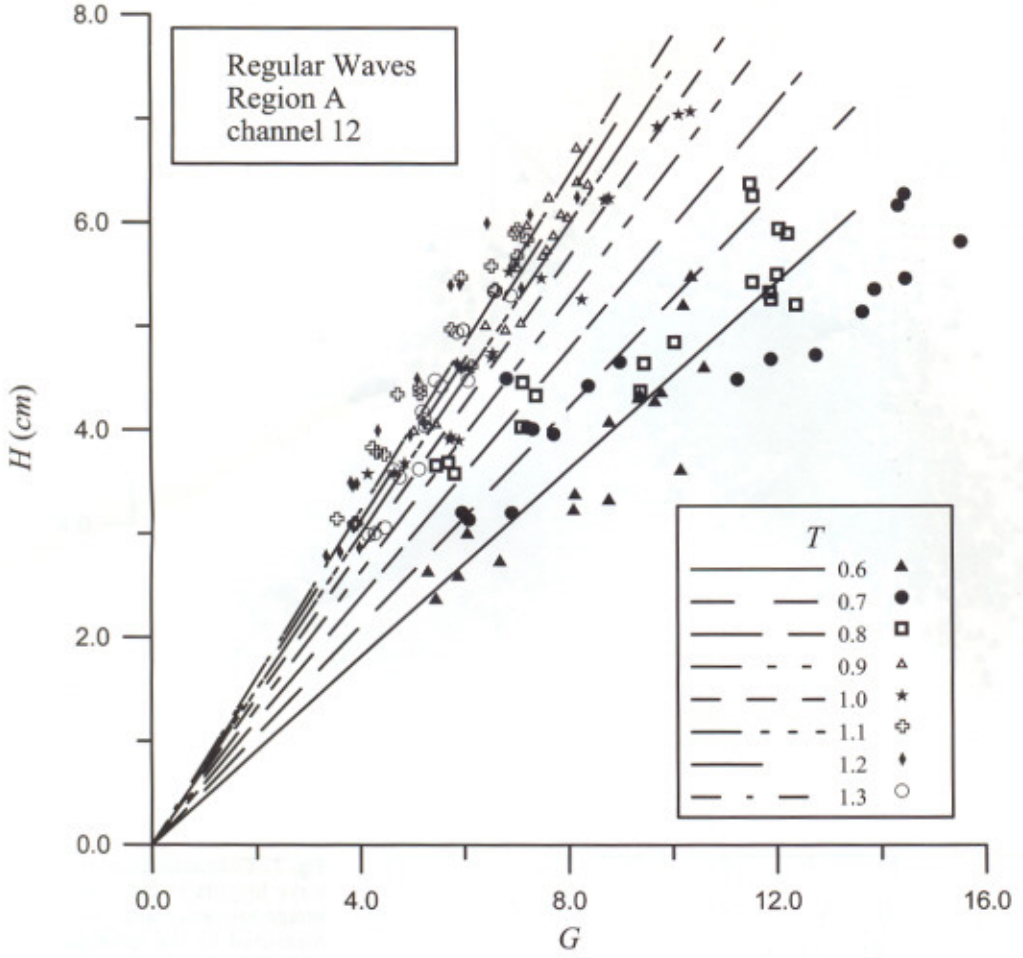

Fig. 8. Relationship between the amplitude of gray value series and the wave height channel 12

estimating wave heights, and the relative errors do not increase with the change of the observed regions. It can be shown that the mean relative error between the estimated and measured wave heights is 0.159. This means that our transform function can be used for different regions in the basin without any further modification.

Figures 8 and 9 compare estimated wave heights from the gray values with measured wave heights by wave gauges of, respectively, channel 12 and channel 27. These channels were on the second line of the wave gauge array located in Region A. In both figures, values estimated through the transfer function are drawn as solid lines; whereas, the symbols are results from wave gauges. It can be seen that for the same "amplitude", G, estimated wave heights increase with increasing values of the periods. Similar trends are also seen for the wave heights of the wave gauges. This means that the "amplitudes" (G) depend not only on the values of the wave heights, but on wave periods as well. It can also be seen that the differences between estimated and measured wave heights are larger for channel 27 than channel 12. Furthermore, it can also be seen that values obtained through the transfer function often underestimate the true values, as a rule.

There are several possible reasons for the biases. Some of the possible causes are: insufficient light sources, non-uniform illumination of the test region, as well as distortions of the images by the camera. Jähne and Schults (1992) indicated that the deviations would increase drastically when these combined nonlinearities are present. On the other hand, the deviation will increase when the measuring points taken into consideration toward to the edge region of images. This can be confirmed by the previous results of channel 12 and 27. It can be seen from Fig. 1 that channel 27 is located in the edge of the frame; therefore, the deviations are rather manifest. Here, we tried to delete data of those stations that are near the four ridges of the images for comparisons. In this way, there are only 12 measuring stations left, which means that data from stations 7–9, 12–14, 17–19, and 22–24 are considered. Figure 10 shows the results as obtained using this method of Region A. The mean value for the relative errors of the measured and predicted wave heights is now reduced to 0.121. Following the same methodology, the mean value for the relative errors in Region B can be reduced to 0.125. However, the effective measuring area will thus be reduced. As our objective is to explore the possibility of measuring a relatively large wave field simultaneously, we therefore make the painful choice to retain all the data in the frame.

For the problem of the non-uniform illumination, the time series of the gray values of the selected points have been adjusted using Eq. 3. This will roughly correct the non-uniformness of the illuminations within the test region.

Results estimated by the wave gauge are always point data. On the other hand, the time series of the gray values are obtained from the pixels of the selected points of the image sequences. Even though each pixel in a frame

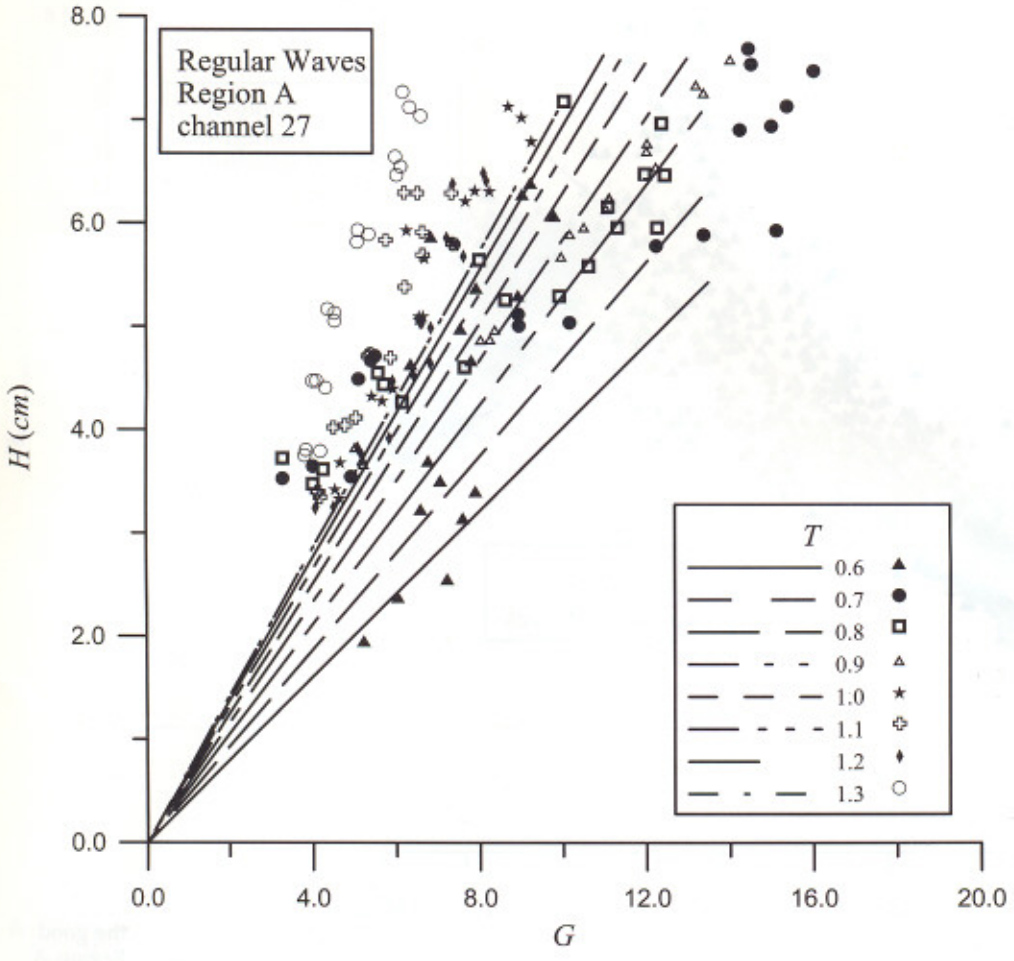

Fig. 9. Relationship between the amplitude of gray value series and the wave height channel 27

appears as a point, it is in reality a small region in the wave basin. A rough estimate shows that a pixel equals a mean area of approximately 4.18 cm^2 in Region A and 3.45 cm^2 in Region B. The actual area occupied by a single pixel in the picture will increase with increasing distance away from the camera. The observed areas in the image will therefore always be larger than those occupied by the wave gauges. It is concluded that this is a possible reason for the bias. A quantitative estimate of this effect has, however, not been carried out thus far.

There is another reason that could also have possibily caused the deviation in our experiment. Experiments with the wave gauge array and those through a CCD camera were not conducted simultaneously. This is because if these were done concurrently, the images of the wave gauges will also be recorded by the CCD camera, and these would further degrade the quality of the images to be analyzed. Although the experimental conditions are the same for both sets of experiments, and we have tried to match the positions of the wave gauges in the image plan as precise as possible, it must be admitted, however, some deviations can still exist and are unavoidable.

4.2
Irregular waves

For the cases of irregular waves, the time series of the gray values were first zero-upcrossed. In the results for a large number of "heights", each associated with its own "wave periods"—usually the number is above 120. All these "waves" are then treated individually, with the transfer function applied to them, and a series of wave heights was thereby obtained.

In Fig. 11 we have plotted the significant wave heights estimated by the wave gauges and those from the image sequences of Region A and B. In this figure, the triangles represent the results from Region A; whereas, the circles are those from Region B. A solid line with a 45° inclination is also shown in the graph. It is seen that even for the irregular waves, estimated wave heights are still distributed closely around the solid line. It can be shown that the mean values of the relative error are, respectively, 0.108 for Region A, and 0.11 for Region B. These values are smaller than those for regular waves. The results seem to indicate that this transfer function can be used directly for the estimation of wave heights of an irregular wave field, and that no further calibrations are necessary. More experimental evidence, however, is necessary to substantiate this conjecture.

In Figs. 12a and 13a we show sections of the time series of the gray values of, respectively, channels 4 and 29; Figs. 12b and 13b are the corresponding dimensionless spectra. Note that since the energies of the frequency spectra of the gray values and wave profiles are in different scales, and in order to make them comparable, we have used their respective peak spectral densities for

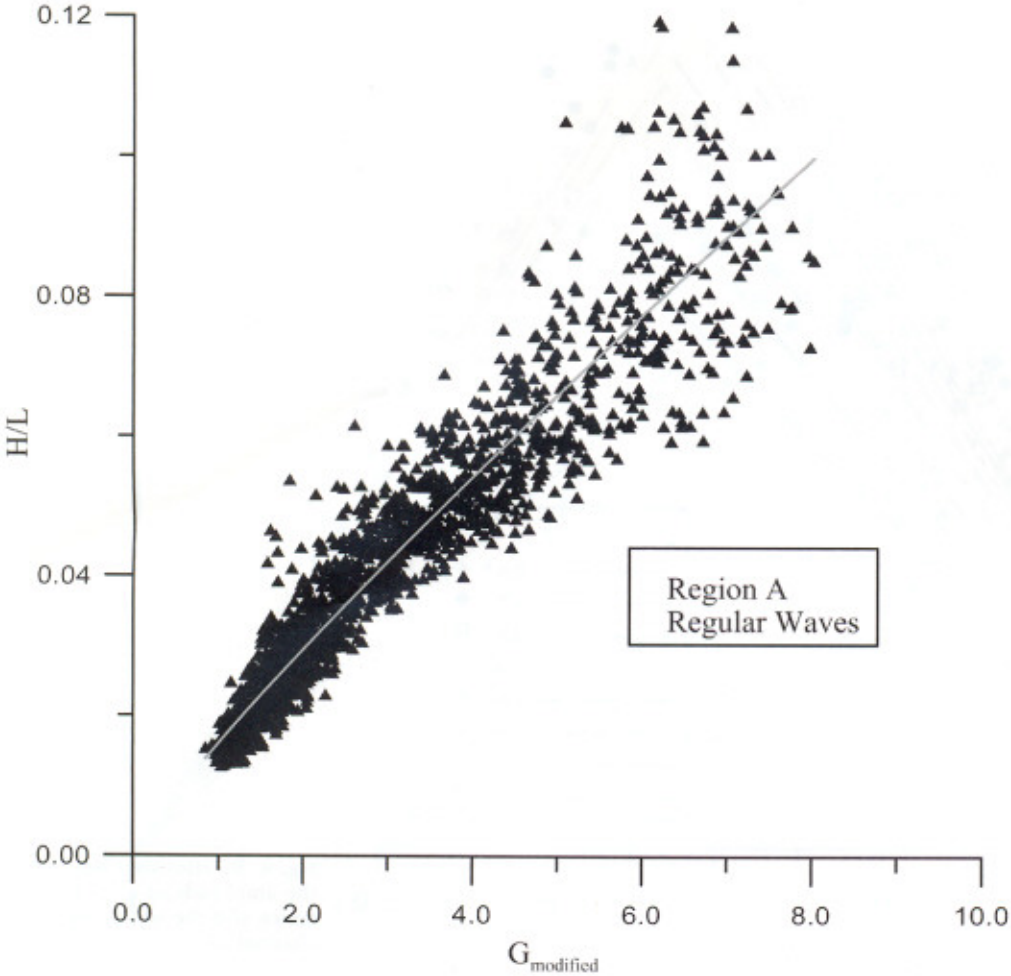

Fig. 10. Results of the goodness-of-fit test for Region A

normalization. Generated waves should have a significant wave height, $H_{1/3}$, of 3.3 cm, with a significant wave period, $T_{1/3}$, of 0.8 s. It can be seen that the peak frequencies estimated from the time series of the image sequences coalesce with those of the wave gauges. This can be treated as a proof of the statement made before, i.e., wave periods can be estimated correctly from image sequences.

It can be seen from Fig. 11b that the two normalized spectra of channel 4 are similar in shape. On the other hand, for channel 29, Fig. 12b, it is seen that for frequencies higher than the spectral peak, the spectrum from the image sequence departs from that from the wave gauge. The spectrum from the image sequence is seen to have more energy than that from wave gauge. Similar findings were also reported by Holthuijsen (1981). A plausible explanation offered by him is that there is a relatively high noise level contained in the images. It can be shown that the mean value of the gray value is 144.83 for channel 4; whereas, it is 122.38 for channel 29. This means that the intensity of the illumination is stronger for the former than the latter. It was often found that there are small-scale high frequency oscillations at both the peaks and valleys of the gray value series. For clarity, we have marked them with elliptic curves in both Figs. 12a and 13a. This is seen to occur more frequently for channel 29 (Fig. 13a) than for channel 4 (Fig. 12a). It is conjectured that the very existence of these small oscillations gives rise to the high frequency part of the spectrum. That is to say, with a dim illumination the oscillations of the water surface cannot be clearly recorded. As a result, zigzagged curves are seen in the series of the gray values. Further smoothing or windowing should be helpful in reducing these irregularities. This has, however, not been carried out in the present study.

5 Conclusions

A series of experiments were carried out. These have the purpose to test the feasibility of using video cameras for large-scale experiments. In this paper we have developed a measured system which uses a CCD camera to sense the wave field characteristics. It is shown that the regions of interest can be extended as compared with previous studies. Compared with the more conventional methods, the advantage of a CCD camera is in its ability of acquiring the information of the whole wave field at one instant. Furthermore, the cameras can be mounted with relative ease. The validity and accuracy of the methods were verified by comparing them with the results of the "in-situ" measurements of the wave gauges. It is encouraging to find that wave periods estimated through the image sequences match those measured by the wave gauges. In addition, it is found that the mean relative errors between these two wave heights are, respectively, less than 0.16 for the case of

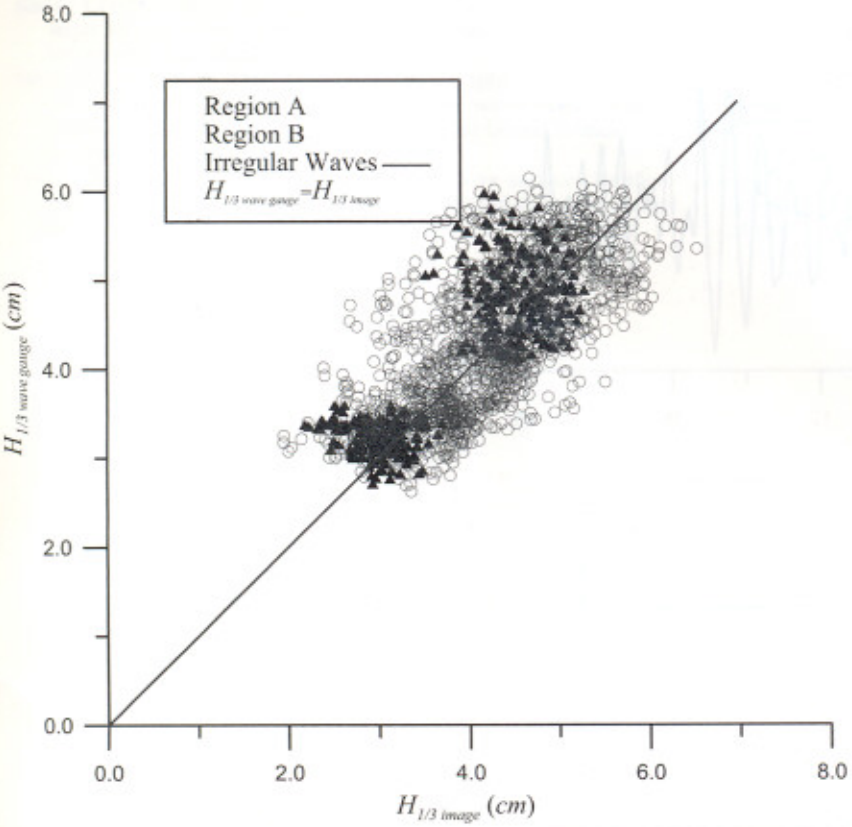

Fig. 11. Results of the goodness-of-fit test for Regions A and B

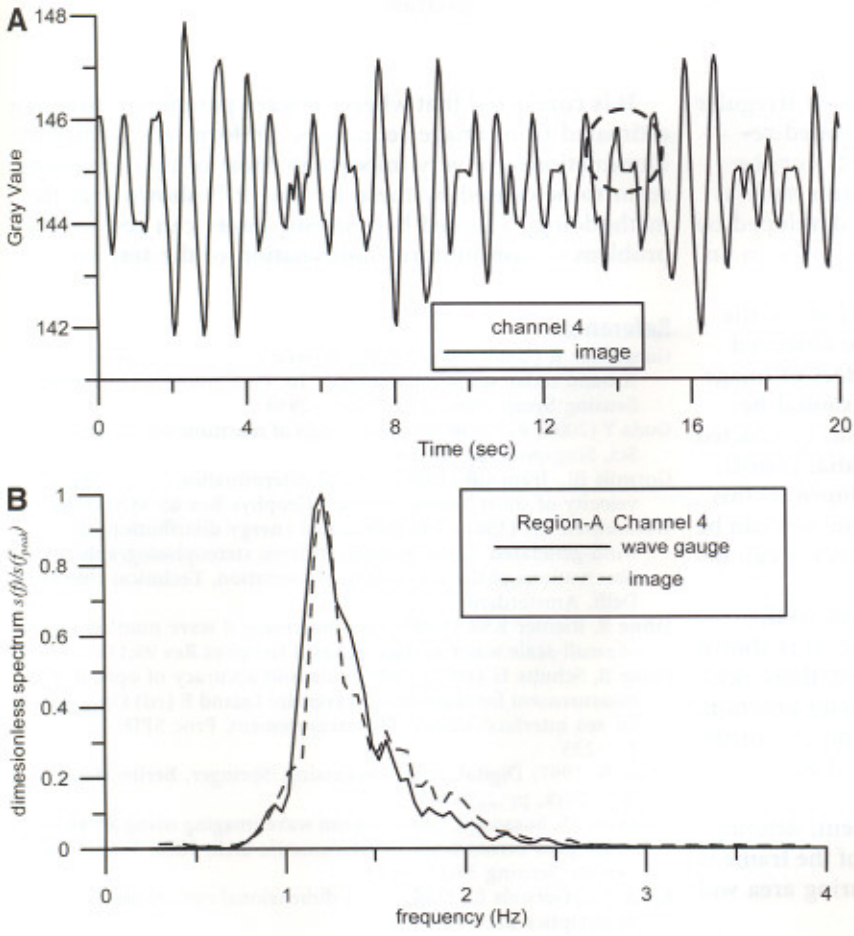

Fig. 12A, B. Channel 4. A Time series of the gray values. B Corresponding dimensionless spectrum

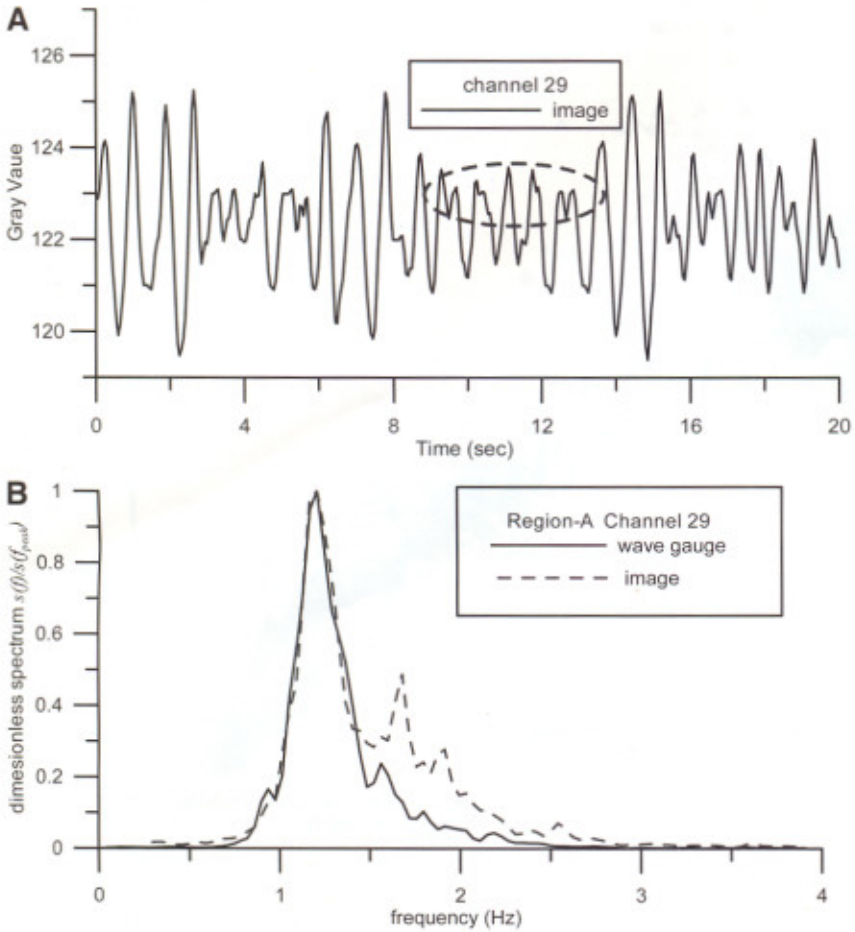

Fig. 13A, B. Channel 29. **A** Time series of the gray values. **B** Corresponding dimensionless spectrum

regular waves, and less than 0.11 for the case of irregular waves. Comparing our relative errors with related research, such as Jähne and Schults (1992) (0.21) or the commercial usage of similar measuring systems such as WaMoSII (*Wa*ve *Mo*nitoring *S*ystem) (0.10) developed by the German GKSS Institute, our results seem to be in an acceptable range.

When analyzing the image sequence of waves in the wave number domain, the dimensions of the observed region should be known beforehand. The effect of image distortions caused by the tilt of the camera should be corrected. The methodology proposed here was conducted in the time domain and did not take the spatial coordinates into consideration. From the results shown in this paper, the procedure of estimating wave parameters can be conducted with relative ease, and the instruments can be mounted in a more flexible way.

A transfer function between the parameters of the images and the wave heights has been derived. It is shown that even if the observing region were changed, there is no need for any further recalibration of this transfer function. It was also found that for the same "amplitude", G, of the gray value, the derived wave heights increased with increasing periods.

For increasing the accuracy of measurement, deleting the data of the measuring points in the edge of the frame is recommended. However, the effective measuring area will thus be reduced.

It is concluded that when the wave parameters are to be estimated from image sequences, uniform and sufficient illuminations are very important. Most of the deviations seem to be caused by these factors. It is shown that the methodology adopted here in this paper can resolve the problem of non-uniform illumination of the test area.

References

Gangeskar R (2000) Wave height derived by texture analysis of X-band radar sea surface images. In: Proc Int Geosci Remote Sensing Symp 2000, IEEE 7:2952–2959

Goda Y (2000) Random seas and design of maritime structures. World Sci, Singapore, pp 28–29

Gotwols BL, Irani GB (1980) Optical determination of the phase velocity of short gravity waves. J Geophys Res 85:3870–3964

Holthuijsen LH (1981) The directional energy distribution of wind-generated waves as inferred from stereophotographic observations of the sea surface. Dissertation, Technical University Delft, Amsterdam

Jähne B, Riemer KSR (1990) Two-dimensional wave number spectra of small-scale water surface waves. J Geophys Res 95:11531–11546

Jähne B, Schults H (1992) Calibration and accuracy of optical slope measurement for short wind waves. In: Leland E (ed) Optics of the air-sea interface: theory and measurement. Proc SPIE 1749, pp 222–233

Jähne B (1997) Digital image processing. Springer, Berlin Heidelberg New York, pp 289–341

Johannes SS, Susanne L (2001) Ocean wave imaging using an airborne single pass across-track interferometric SAR. IEEE Trans Geosci Remote Sensing 39(1):38–45

Keller KC, Gotwols BL (1983) Two-dimensional optical measurement. Appl Optics 22:3476–3478

Klinke J (1996) Optical measurement of small-scale wind-generated water surface waves in the laboratory and the field. Dissertation, University of Heidelberg
Senet CM, Seemann J, Zimer F (2000a) Hydrographic parameter maps deduced from CCD image sequences of the water surface supplement by in-situ wave gauges. In: Proc Int Geosci Remote Sensing Symp 2:843–846
Senet CM, Seemann J, Zimer F (2000b) Dispersive surface classification: Local analysis of optical image sequences of the water surface to determine hydrographic parameter maps. In: Oceans 2000 MTS/IEEE Conf Exhib 3:1769–1774
Stilwell D Jr, Pilon RO (1974) Directional spectra of surface waves from photographs. J Geophys Res 79:1277–1284
Sugimori Y (1975) A study of the application of the holographic method to the determination of the directional spectrum of the ocean waves. Deep-Sea Res 22: 339–350
WaMoSII: Technical data sheet and system requirement and benefits. http://www.oceanwaves.de/technicals.htm
Young IR, Rosenthal W, Ziemer F (1985) A three-dimensional analysis of marine radar images for the determination of ocean wave directionality and surface currents. J Geophys Res 90:1049–1059